Atmospheric
Measurement
Techniques
Open Access
Discussions

The use of NO_2 absorption cross section temperature sensitivity to derive NO_2 profile temperature and stratospheric/tropospheric column partitioning from visible direct sun DOAS measurements

E. Spinei[1,2], A. Cede[3,2], W. H. Swartz[4,2], J. Herman[5,2], and G. H. Mount[6]

[1]ESSIC, University of Maryland, College Park, MD, USA
[2]NASA/Goddard Space Flight Center (GSFC), Greenbelt, MD, USA
[3]Universities Space Research Association, Greenbelt, MD, USA
[4]Applied Physics Laboratory, The Johns Hopkins University, Laurel, MD, USA
[5]University of Maryland, Baltimore County (UMBC), Catonsville, MD, USA
[6]Laboratory for Atmospheric Research, Washington State University (WSU), Pullman WA, USA

Discussion Paper | Discussion Paper | Discussion Paper | Discussion Paper |

AMTD

7, 5695–5740, 2014

NO_2 direct sun DOAS measurements

E. Spinei et al.

Title Page

Abstract | Introduction

Conclusions | References

Tables | Figures

|◄ | ►|

◄ | ►

Back | Close

Full Screen / Esc

Printer-friendly Version

Interactive Discussion

Title Page

Abstract | Introduction

Conclusions | References

Tables | Figures

|◄ | ►|

◄ | ►

Back | Close

Full Screen / Esc

Printer-friendly Version

Interactive Discussion

Abstract

This paper presents a TEmperature SEnsitivity Method (TESEM) to accurately calculate total vertical NO_2 column, atmospheric slant NO_2 profile-weighted temperature (T), and to separate stratospheric and tropospheric columns from direct-sun (DS) ground-based measurements using the retrieved T. TESEM is based on Differential Optical Absorption Spectroscopy (DOAS) fitting of the linear temperature-dependent NO_2 absorption cross section, σ (T), regression model (Vandaele et al., 2003). The direct result of the DOAS spectral fitting retrieval is NO_2 differential slant column density (ΔSCD) at the actual atmospheric NO_2 T. Atmospheric NO_2 T is determined from the DOAS fitting results after SCD in the reference spectrum is estimated using the Minimum Langley Extrapolation method (MLE).

Since NO_2 is mostly distributed between the lower troposphere and middle stratosphere and direct sun measurements have almost equal sensitivity to stratospheric and tropospheric absorption at solar zenith angles < 75° with a well known photon path, we assume that the retrieved total column NO_2 T can be represented as a sum of the NO_2 stratospheric and tropospheric Ts multiplied by the corresponding stratospheric and tropospheric fractions of the total SCD_{NO_2}. We use Global Modeling Initiative (GMI) chemistry–transport model (CTM) simulations to evaluate diurnal and seasonal variability of stratospheric and tropospheric NO_2 T over two northern middle latitude sites in 2011. GMI simulations reveal that stratospheric NO_2 T over northern middle latitudes can be estimated with an error of less than 3 K by the simulated temperature at 27 km from April to October. During November–March months the error can reach as high as 10 K. The tropospheric NO_2 T can be approximated by the surface temperature within 3–5 K according to GMI simulations.

Traditionally, either σ (NO_2) is fitted at a single estimated NO_2 T, or two predetermined (stratospheric and tropospheric) temperatures. Use of a single T requires prior knowledge of the tropospheric–stratospheric NO_2 columns partitioning in the measurement. In addition, it assumes that this partitioning is constant throughout the

measurement period (sometimes months). Fitting of two σ (NO$_2$) at fixed temperatures, typically 220 and 298 K, assumes constant stratospheric and tropospheric NO$_2$ T as a function of time. Neither assumption is correct, except as a convenient approximation. TESEM does not require prior knowledge of NO$_2$ effective temperatures during the DOAS fitting stage and retrieves T from the DOAS fitting results themselves.

TESEM was applied to the Washington State University Multi Function DOAS instrument (MFDOAS) measurements at four mid-latitude locations with low and moderate NO$_2$ anthropogenic emissions: (1) Table Mountain – Jet Propulsion Laboratory (JPL-TMF) facility, CA (34.38° N/117.68° W); (2) Pullman, WA (46.73° N/117.17° W); (3) Greenbelt, MD (38.99° N/76.84° W) USA; and (4) Cabauw, the Netherlands (51.97° N/4.93° E) during summer months (July 2007, June–July 2009, July–August 2011, May 2013). NO$_2$ T, total, stratospheric and tropospheric NO$_2$ vertical columns were determined over each site.

1   Introduction

1.1   NO$_2$ importance

Active nitrogen oxides (NO$_x$ = NO + NO$_2$) play an important role in atmospheric chemistry. They catalyze ozone destruction in the stratosphere, activate ozone production in the lower troposphere, and influence the HO$_x$ budget. NO$_2$ itself is an air toxin affecting human health and is a precursor of acid rain in the lower troposphere (Mohnen, V.A., 1988). As a result, the vertical distribution of NO$_2$ and its temporal variability is of great interest.

The main source of NO$_x$ in the stratosphere is nitrous oxide (N$_2$O) transported from the troposphere, where about 10 % of N$_2$O is converted to NO$_x$. Stratospheric NO$_2$ concentrations greatly depend on the solar actinic flux available for the NO$_x$ reservoir and NO$_2$ photolysis. N$_2$O$_5$ is the most important nighttime off-polar NO$_x$ reservoir.

Tropospheric NO$_x$ mainly arises from fossil fuel combustion (vehicular, industrial, and air traffic), biomass burning (natural and anthropogenic), soil microbial production, lightning, and ammonia oxidation. Anthropogenic sources account for $\sim 75\%$ of total global emissions with a large uncertainty of $\sim 40\%$ (Olivier et al., 1998). Vehicular emissions are estimated to contribute up to 50 % of total NO$_x$ emissions and are characterized by high heterogeneity in space and time.

NO$_x$ is efficiently removed from the lower troposphere (lifetime 3–10 h in the tropics and summer northern mid-latitudes, increasing to 48 h in winter at high latitudes) mainly by wet and dry deposition of HNO$_3$ (Martin et al., 2003). The NO$_x$ lifetime in the free troposphere is longer (5–10 days) mainly due to lower humidity levels (Wenig et al., 2003). The lower troposphere NO$_x$ lifetime allows for transport on a regional scale (up to 100 km). Long range transport of NO$_x$ introduced into the free troposphere from the planetary boundary layer (PBL) has also been observed (Parrish et al., 2004; Wenig et al., 2003).

1.2 NO$_2$ atmospheric profile modeling

Figure 1 shows an example of NO$_2$ winter and summer vertical profiles estimated by the Global Modeling Initiative (GMI) chemistry–transport model (CTM) (Duncan et al., 2007; Strahan et al., 2007) for the rural north-west USA (46° N/117.5° W) in 2011. GMI simulations of diurnal and seasonal variability of stratospheric NO$_2$ column amounts are also shown in Fig. 2. Slow photolysis of N$_2$O$_5$ is responsible for the gradual increase in stratospheric NO$_2$ concentrations during the day. After sunset, stratospheric NO$_2$ concentrations rise sharply to their maximum due to NO oxidation by O$_3$. The NO$_2$ concentrations then gradually fall during the course of the night with a corresponding increase in N$_2$O$_5$ concentrations. After sunrise, stratospheric NO$_2$ sharply drops to its minimum due to photolysis. The seasonal variability of stratospheric NO$_2$ is also governed by the seasonal change in actinic flux (photolytic release of NO$_2$ from NO$_x$ reservoirs). GMI-CTM model calculations show that maximum columns are expected in summer and minimum in winter. Photolysis rates also define the altitude of

the stratospheric NO_2 peak and its width (Fig. 1). The stratospheric NO_2 distribution tends to be broader in altitude in summer compared to winter.

1.3 Differential optical absorption spectroscopy

Passive differential optical absorption spectroscopy (DOAS) has been successfully applied since the 1970s to retrieve numerous trace gases, including NO_2, from ground-based and satellite instruments (Noxon, 1975, 1979; Mount, 1987; Solomon et al., 1987; Platt, 1979, 1994; Plane and Smith, 1995). While all passive DOAS measurements contain information about gas absorption at all atmospheric altitudes, different observation geometries have been developed to optimize the sensitivity of the passive DOAS instruments to trace gas amounts located in various layers of the atmosphere.

The "traditional" ground-based DOAS technique employs a zenith looking instrument to measure scattered sunlight (Noxon, 1975, 1979), and is mainly sensitive to stratospheric and upper tropospheric absorbers, especially at large solar zenith angles (SZA > 85°). Vertical stratospheric NO_2 profiles during sunset/sunrise were derived from zenith sky (e.g. McKenzie et al., 1991; Preston et al., 1997; Hendrick et al., 2004), and balloon DOAS measurements (e.g. Pommereau and Piquard, 1994; Butz et al., 2006; Kritten et al., 2010). Sunset and sunrise stratospheric NO_2 columns have been measured since 1991 at multiple locations throughout the world as part of the international Network for the Detection of Atmospheric Composition Change (NDACC) (Hendrick et al., 2011). Sunrise/sunset NO_2 vertical columns are typically interpolated to daylight hours using chemical transport models (Hendrick et al., 2004).

In the past two decades, ground-based multi-axis DOAS (MAX-DOAS) techniques have been developed, measuring scattered sunlight at multiple low elevation angles (Wagner et al., 2004, 2007, 2010; Heckel et al., 2005; Frieß et al., 2006; Sinreich et al., 2005; Li et al., 2008, 2010, 2013; Irie et al., 2008, 2009; Clémer et al., 2010). In contrast to the zenith DOAS, MAX-DOAS has significant sensitivity to tropospheric gas absorption due to increased photon path length through the lower troposphere.

NO$_2$ direct sun DOAS measurements

E. Spinei et al.

Title Page

Abstract	Introduction
Conclusions	References
Tables	Figures

◄◄ ►►

◄ ►

Back Close

Full Screen / Esc

Printer-friendly Version

Interactive Discussion

Discussion Paper | Discussion Paper | Discussion Paper | Discussion Paper

Direct-sun/direct-moon (DS/DM) DOAS, is equally sensitive to the stratospheric and tropospheric absorbers at SZA < 80°, and allows for very simple data interpretation (Cede et al., 2006; Herman et al., 2009; Wang et al., 2010; Spinei et al., 2010). This is due to the almost geometric calculation of DS/DM air mass factors (AMF). Compared to MAX-DOAS, it has a lower overall absorption sensitivity (Brewer et al., 1973; Cede et al., 2006) because of shorter path length in the atmosphere.

The DOAS technique is based on the modified Beer–Lambert law, which describes the spectral attenuation of electromagnetic radiation by molecular and aerosol absorption and scattering. DOAS retrieval consists of two steps. In the first step, spectral evaluation, differential slant column densities (ΔSCD) of the species of interest are calculated. This step is accomplished through simultaneous nonlinear least-squares spectral fitting of differential slant optical depths (τ) from various molecular and "pseudo" absorbers (e.g., Ring effect), a low-order polynomial (3–5) function, and an offset to the difference between the logarithms of the attenuated and reference spectra. The Fraunhofer line intensity of scattered solar light is not constant (Grainger and Ring, 1962). Up to a several percent decrease in the line depth and line broadening is observed compared to the direct sun spectra. This phenomenon is called the Ring effect and is mostly attributed to the rotational Raman scattering by the air molecules (N_2 and O_2) (Kattawar et al., 1981; Fish and Jones, 1995; Chance and Spurr, 1997). To account for variability of the Fraunhofer line intensity, a Ring spectrum is fitted as a "pseudo" absorption cross section during the DOAS analysis. The second step of the analysis is conversion of the ΔSCD into the vertical column density (VCD) of the molecular absorbers. Exact implementation of this last step depends on the observation geometry (e.g. DS, MAX or zenith).

NO_2 ΔSCD is typically retrieved from visible DOAS measurements in the 400–500 nm wavelength range, where the larger spectral structure gives the greater sensitivity to NO_2 absorption. The oxygen collision complex (O_2O_2), water (H_2O) and O_3 also show spectrally varying absorptions in this wavelength window. Since spectral attenuation by NO_2 and O_3 takes place at different altitudes with different atmospheric

Printer-friendly Version

Interactive Discussion

temperatures, cross sections must be fitted at the corresponding slant profile weighted (effective) temperatures, T. These T are determined from the NO$_2$ volume mixing ratio profile (VMR) weighted by the air density profile in each atmospheric layer and average layer temperature from the bottom of the atmosphere (BOA) to the top of atmosphere (TOA). On most occasions, gas effective temperature along the photon path is not known. Traditionally, either NO$_2$ cross sections at a single profile weighted temperature or two (stratospheric: 220 K and tropospheric: 298 K) temperatures are fitted. Usually, constant tropospheric and stratospheric temperatures are assumed throughout the measurement period. While this is never true during an extended observation period, it is used as a convenient approximation.

Accurate ground based DOAS measurements are crucial for validation of NO$_2$ satellite observations and estimates from chemistry–transport models (CTM). This paper presents a simple temperature sensitivity method (TESEM) to calculate NO$_2$ slant profile-weighted temperature, T, and total NO$_2$ VCD at T, and to separate stratospheric and tropospheric NO$_2$ VCD from DS DOAS ground-based visible wavelength observations. TESEM is demonstrated using Washington State University Multi Function DOAS instrument (MFDOAS) measurements at four locations at middle latitudes: Table Mountain – Jet Propulsion Laboratory (JPL) facility, CA (34.38° N/117.68° W); Pullman, WA (46.73° N/117.17° W); Greenbelt, MD (38.99° N/76.84° W); USA and Cabauw, the Netherlands (51.97° N/4.93° E), see Table 1) during summer months.

The paper is organized in the following sections. Section 2 describes NO$_2$ cross section temperature dependence and DOAS retrieval of ΔSCD at the slant profile weighted temperature. Section 3 lays out background for temperature sensitivity method to separate stratospheric and tropospheric NO$_2$ SCDs based on the derived NO$_2$ slant profile weighted temperature. Section 4 evaluates stratospheric and tropospheric NO$_2$ T using NO$_2$ profile simulations by GMI CTM. Section 5 summarizes TESEM and discusses its limitations. Section 6 briefly describes the MFDOAS instrument and measurements used in this study. Section 7 presents results from four field campaigns with moderate-high and low NO$_2$ pollution levels. Section 8 focuses on conclusions.

2 Retrieval of total NO$_2$ ΔSCD based on a linear NO$_2$ temperature dependent absorption cross section model.

NO$_2$ is distributed at different altitudes from surface to upper stratosphere. As a result, passive DOAS instruments measure net attenuation of solar radiation by NO$_2$ at significantly different temperatures. The cumulative absorption optical depth for a specific DOAS observation geometry can be described in terms of the NO$_2$ profile-weighted temperature along an average photon path (slant T). Since passive DOAS observations contain this "built-in" information about T, accurate retrieval of NO$_2$ ΔSCD requires knowledge of slant T.

Investigation of the temperature sensitivity of NO$_2$ absorption in zenith sky measurements was first initiated by J. Noxon in the late 1970's and early 1980's (unpublished data). However, due to the low quality of the scanning grating instruments at that time, deriving NO$_2$ temperature dependence information from scattered sky measurements was not possible. As the scientific understanding of the radiative transfer improved (e.g., modeling of Ring spectra) along with the development of better instrumentation utilizing multiplexing detectors (photodiode arrays and CCDs) and availability of higher quality molecular absorption cross section laboratory measurements, fitted DOAS optical depth spectral residuals decreased to near the photon shot noise limits ($< 5 \times 10^{-4}$). At these low residual levels zenith sky and MAX-DOAS measurements indeed reveal NO$_2$ temperature sensitivity. This encouraged high quality laboratory measurements of NO$_2$ cross sections in the UV and visible parts of spectrum at different temperatures from 220 K to room temperatures (Harder et al., 1997; Vandaele, 1998). However, these laboratory NO$_2$ absorption cross sections at 220 K and room temperature show high cross correlation. This cross correlation introduces errors in derived ΔSCD due to instrumental noise and uncertainties in all fitted cross sections. Richter (1997) suggested reducing cross correlation through cross section "orthogonalization" by means of the Graham–Smith process. Where an "orthogonalised" cross section at one temperature T_1, σ^{ortho} ($T_1 \rightarrow T_2$), relative to the cross section at a second temperature

T_2 (σ_{T_2}), is equal to σ_{T_1} minus σ_{T_2} multiplied by a scaling factor (SF). SF is numerically equal to the "DOAS fit value" of σ_{T_2} "into" σ_{T_1} in a specific fitting wavelength window. Simultaneous spectral fitting of σ^{ortho} ($T_1 \rightarrow T_2$) and σ_{T_2} results in an approximation of the "true" ΔSCD at T_1 from σ^{ortho} ($T_1 \rightarrow T_2$) fit. While ΔSCD from σ_{T_2} fitting, ΔSCD(σ_{T_2}), is equal to approximations of ΔSCD at T_2 plus ΔSCD at T_1 multiplied by SF (ΔSCD(σ_{T_2}) = ΔSCD$_{T_2}$ + ΔSCD$_{T_1}$·SF). Richter (1997) fitted σ_{221} and σ^{ortho}(293 → 221) to derive tropospheric and stratospheric absorptions from zenith sky measurements using modified Langley–Plot method.

We propose to derive slant T and ΔSCD at T from DOAS observations by fitting the NO$_2$ cross section temperature dependence model.

2.1 NO$_2$ cross section temperature dependence

The temperature dependent NO$_2$ cross section, σ, in UV and visible wavelength regions can be calculated at any T, using a linear regression model (Vandaele et al., 2003) (Eq. 1).

$$\sigma(\lambda, T) = \sigma_0(\lambda) + \alpha(\lambda) \cdot (T - T_0) \tag{1}$$

Where the constant, $\sigma_0(\lambda)$ is the NO$_2$ absorption cross section [cm^2 molecule^{-1}] at temperature T_0 and wavelength λ; and $\alpha(\lambda)$ is a temperature dependent coefficient describing the change of NO$_2$ absorption cross section [cm^2 (K molecule)$^{-1}$] with temperature at wavelength λ. Figure 3 shows the high resolution (0.1 cm^{-1}, Vandaele et al., 2003) laboratory $\sigma_0(\lambda)$ at 273 K and $\alpha(\lambda)$ convolved with the MFDOAS instrument transfer function (FWHM 0.83 nm/40.91 cm^{-1} at 450 nm). While the atmospheric NO$_2$ profile spans an altitude range with a significant pressure gradient, the pressure effect on $\sigma(\lambda)$ is not present at spectral resolution $\Delta\lambda > 2$ cm^{-1} (0.04 at 450 nm; Vandaele et al., 2003). Since most DOAS systems have much lower spectral resolution ($\Delta\lambda > 0.4$ nm/FWHM), the effect of pressure is ignored in this analysis.

2.2 NO$_2$ slant column density at NO$_2$ profile weighted temperature

To improve the retrieval of NO$_2$ ΔSCD from passive DOAS measurements, which are simultaneously affected by both stratospheric and tropospheric temperature regimes, we can derive slant NO$_2$ T from the DOAS measurements themselves by fitting σ linear regression model parameters $\sigma_0(\lambda)$ and $\alpha(\lambda)$. To simplify further notation we assign $T_0 = 0\,^\circ$C and omit reference to λ.

The Beer–Lambert law written for a single absorber, NO$_2$, with linear temperature dependent $\sigma(T)$ and ideal ground based DOAS measurements of solar monochromatic light is described according to Eq. (2):

$$
\ln\left(\frac{I^{\text{REF}}}{I}\right) = \tau - \tau^{\text{REF}} = \text{SCD} \cdot [\sigma_0 + \alpha \cdot T] - \text{SCD}^{\text{REF}} \cdot \left[\sigma_0 + \alpha \cdot T^{\text{REF}}\right]
$$

$$
= \sigma_0 \cdot \underbrace{\Delta\text{SCD}}_{\text{DOAS fit result}} + \alpha \cdot \underbrace{[\text{SCD}^{\text{REF}} \cdot (T - T^{\text{REF}}) + \Delta\text{SCD} \cdot T]}_{\text{DOAS fit result}} \tag{2}
$$

Where, I and I^{REF} are the measured intensities of an attenuated and a reference spectrum [counts/sec] at wavelength λ [nm]; SCD and SCD$^{\text{REF}}$ are slant column densities of NO$_2$ along an average photon path at observation and reference times respectively [molecules cm^{-2}]; T and T^{REF} are NO$_2$ slant profile weighted temperatures at the observation and reference times respectively [K]. The photon path for each direct sun measurement is described by an air mass factor (AMF) and is defined by solar zenith angle, Earth surface curvature and, to a smaller degree, NO$_2$ profile (at SZA > 75°, Cede et al., 2006).

For an ideal DOAS instrument and analysis, a reference spectrum is an extraterrestrial solar spectrum convolved with the instrument transfer function. In practice, a spectrum taken from the surface with the DOAS instrument is used to allow detection of optically thin absorbing species (e.g., NO$_2$) above the instrumental errors. Reference spectra are typically measured at the observation conditions with minimum photon path

and NO_2 total column. Measured this way, the reference spectrum contains absorption by NO_2 at the reference observation conditions. Therefore, the DOAS spectral fitting determines differential SCD (ΔSCD) at T, which is the difference between the SCD present at the observation and reference conditions.

Simultaneous DOAS fitting of optical depth due to σ_0 and α results in ΔSCD at the slant T and $\Delta\text{SCD}T_\alpha = [\text{SCD}^{\text{REF}} \cdot (T - T^{\text{REF}}) + \Delta\text{SCD} \cdot T]$ respectively. This is an improvement on the currently used DOAS assumptions (see introduction), since no prior assumption is made about the stratospheric/tropospheric NO_2 profile partitioning or temperatures during the DOAS fitting step. Derived $\Delta\text{SCD}T_\alpha$ is simply related to T.

2.3 NO_2 slant profile-weighted temperature

NO_2 profile-weighted T is an important quantity on its own, since it carries information about both tropospheric and stratospheric contributions. It can be determined from the DOAS fitted optical depth of the temperature coefficient, $\Delta\text{SCD}T_\alpha$, as defined in Eq. (3a):

$$T = \frac{\Delta\text{SCD}T_\alpha + \text{SCD}^{\text{REF}} \cdot T^{\text{REF}}}{\Delta\text{SCD} + \text{SCD}^{\text{REF}}} \tag{3a}$$

SCD^{REF} and T^{REF} are not known beforehand. Under certain conditions $\text{SCD}^{\text{REF}} \ll \Delta\text{SCD}$ and Eq. (3a) simplifies to Eq. (3b):

$$T \approx \frac{\Delta\text{SCD}T_\alpha}{\Delta\text{SCD}} \tag{3b}$$

The condition of $\text{SCD}^{\text{REF}} \ll \Delta\text{SCD}$ holds when the reference spectrum is chosen at the smallest SZA and lowest pollution level compared to the rest of the measurements and the measurements are made at large solar zenith angles. SCD^{REF} and T^{REF} can be estimated from the DOAS measurements themselves knowing T if stratospheric and tropospheric SCD at the reference time can be approximated.

3 Separation of stratospheric and tropospheric NO$_2$ SCDs based on the derived NO$_2$ slant profile-weighted temperature

Since vertical NO$_2$ profile has mostly bimodal shape at distinctly different temperatures and altitudes, total slant NO$_2$ T can be approximated as a sum of the stratospheric and tropospheric slant Ts (T^{STRAT} and T^{TROP}) multiplied by their corresponding total column fractions (χ, Eq. 4).

$$T = \chi_{STRAT} \cdot T^{STRAT} + \chi_{TROP} \cdot T^{TROP} = \chi_{STRAT} \cdot T^{STRAT} + (1 - \chi_{STRAT}) \cdot T^{TROP} \qquad (4)$$

After rearranging Eq. (4) we can estimate stratospheric (χ_{STRAT}) and tropospheric (χ_{TROP}) fractions of total SCD:

$$\chi_{STRAT} = \frac{T - T^{TROP}}{T^{STRAT} - T^{TROP}} \qquad (5)$$

Note, χ_{STRAT} is very sensitive to derived T and assumed tropospheric and stratospheric T over clean sites (large χ_{STRAT}). Stratospheric and tropospheric SCD are subsequently determined by multiplying their corresponding fractions by the total SCD.

$$SCD^{STRAT} = SCD \cdot \chi_{STRAT}; SCD^{TROP} = SCD \cdot (1 - \chi_{STRAT}) \qquad (6)$$

Equations (3a) and (5) show that accurate separation of stratospheric/tropospheric NO$_2$ column require knowledge of NO$_2$ SCD^{REF} and NO$_2$ T^{REF} in the reference spectrum. SCD^{REF} can be estimated using Minimum Langley extrapolation method (MLE, Eq. (7). Where the slope of the smallest ΔSCD in each AMF bin vs. (AMF-AMF^{REF}) is determined to approximate VCD at the reference time (VCD^{REF}):

$$\Delta SCD = \Delta VCD \cdot AMF + VCD^{REF} \cdot (AMF - AMF^{REF}) \qquad (7)$$

Due to strong changes in NO$_2$ stratospheric VCD at SZA > 75° and the main assumption of MLE that there are data with constant VCD = VCD^{REF} (ΔVCD $\approx$ 0), only measurements at SZA < 75° are used to derive VCD^{REF}.

T^{REF} is harder to estimate since it requires prior knowledge of stratospheric and tropospheric NO_2 SCDs in the reference spectrum. To do this we take advantage of the measurements when $\Delta\text{SCD} \gg \text{SCD}^{\text{REF}}$ (large SZA and pollution levels in case of DS). For such conditions $\text{SCD} \approx \Delta\text{SCD}$ and Eq. (3b) is valid to calculate T. Then stratospheric SCD in the reference spectrum ($\text{SCD}_{\text{REF}}^{\text{STRAT}}$) can be approximated using MLE. Note, that even though derived T has very large errors around the reference measurement time, this has only small impact on tropospheric and stratospheric NO_2 SCD^{REF} estimation. This is because measured ΔSCD around reference time are almost zero and $\text{SCD}_{\text{REF}}^{\text{STRAT}}$ determination using MLE is "driven" by the measurements at larger SZA when Eq. (3b) is valid. After $\text{SCD}_{\text{REF}}^{\text{STRAT}}$ is estimated, the T^{REF} can be determined, knowing stratospheric and tropospheric NO_2 profile T at the reference time ($T_{\text{REF}}^{\text{STRAT}}, T_{\text{REF}}^{\text{TROP}}$)

$$T^{\text{REF}} = \frac{\text{SCD}_{\text{REF}}^{\text{STRAT}} \cdot T_{\text{REF}}^{\text{STRAT}} + (\text{SCD}^{\text{REF}} - \text{SCD}_{\text{REF}}^{\text{STRAT}}) \cdot T_{\text{REF}}^{\text{TROP}}}{\text{SCD}^{\text{REF}}} \tag{8}$$

Accurate calculation of T is now possible for all measurements using Eq. (3a) and subsequent stratosphere–troposphere NO_2 partitioning ($\text{SCD}^{\text{STRAT}}/\text{SCD}^{\text{TROP}}$) using Eq. (5) and (7).

The only unknown parameters in Eq. (5) and (8) are slant T^{TROP}, T^{STRAT}, $T_{\text{REF}}^{\text{STRAT}}, T_{\text{REF}}^{\text{TROP}}$. These slant temperatures are related to vertical profile weighted temperatures through the corresponding tropospheric and stratospheric AMFs ($\text{AMF}^{\text{STRAT}}$ and AMF^{TROP}) normalized by total AMF:

$$T^{\text{STRAT}} = \text{AMF}_{\text{norm}}^{\text{STRAT}} \cdot T_{\text{vertical}}^{\text{STRAT}}, \quad T^{\text{TROP}} = \text{AMF}_{\text{norm}}^{\text{TROP}} \cdot T_{\text{vertical}}^{\text{TROP}} \tag{9}$$

For DS NO_2 measurements there is very little dependence of AMF on λ at most SZAs, therefore, slant T are also wavelength independent.

4 Estimation of NO$_2$ vertical profile weighted temperatures based on GMI CTM simulations

In this section we use NO$_2$ profile simulations from the GMI CTM for two purposes: (1) to evaluate diurnal and seasonal variability of stratospheric and tropospheric vertical NO$_2$ profile weighted temperatures and heights, and (2) to demonstrate that vertical T^{TROP} and T^{STRAT} can be relatively well approximated from measured or modeled temperature profiles at specific altitudes (surface and 27 km). GMI analysis results are shown for the grid cells encompassing Pullman, WA (north-west USA, 46° N/117.5° W) and Cabauw, the Netherlands (north-west Europe, 52° N/5° E).

The GMI CTM simulates the overall state of the stratosphere and troposphere. It accounts for most important chemical and physical processes (emissions, aerosol microphysics, chemistry, deposition, radiation, advection, lightning NO$_x$ production, Duncan et al., 2007). The GMI chemistry couples the stratospheric chemical mechanism described by Douglass et al. (2004) with tropospheric O$_3$-NO$_x$-hydrocarbon chemistry derived from the Harvard GEOS-Chem model (Bey et al., 2001). It is driven by GEOS-5 meteorological fields (Rienecker et al., 2008) at a resolution of 2° (latitude) × 2.5° (longitude). The atmosphere is modeled on a vertical grid from the surface to 0.01 hPa, with 72 levels. Level heights range from ∼ 150 m in the planetary boundary layer to ∼ 1 km in the free troposphere and lower stratosphere. Three-dimensional NO$_2$ fields were saved every hour to account for the diurnal variation of NO$_2$, particularly in the stratosphere. Stratospheric profiles in this study are identified as profiles above 8 km, and tropospheric – below 8 km.

The center of mass of the NO$_2$ profile from GMI CTM simulations can be defined as profile weighted height (H_{eff}), where the NO$_2$ VMR is weighted by the air density profile in each atmospheric GMI grid layer and average layer height. In similar manner T_{eff} is calculated. The subscript of "eff" is used to distinguish vertical modeling results from other parameters. Figure 4 shows examples of stratospheric NO$_2$

H_{eff} and T_{eff} calculated from GMI CTM estimations over north-west USA (cell center: 46° N/117.5° W) for 10 July and 1 December 2011.

Stratospheric NO_2 H_{eff} has very small variability during daylight hours (SZA < 80°) ranging from 25 to 27 km. It tends to be somewhat higher at night (by 1–3 km), with a minimum around sunset/sunrise (Fig. 4). Change in stratospheric T_{eff} during daylight hours is no more than ±1 K during a particular day.

Figure 5 shows stratospheric and tropospheric H_{eff} calculated from GMI estimations for the north-west USA (46° N/117.5° W) with low anthropogenic emissions and for the heavily populated north-west Europe with moderate-to-high NO_2 emissions (52° N/5° E) for year 2011. As expected, tropospheric NO_2 profile H_{eff} is closer to the surface over strong emission sources (52° N/5° E): 0.6 ± 0.2 km. A more homogeneous distribution within the lower troposphere is estimated by GMI CTM over low emission region (46° N/117.5° W): 1 ± 0.4 km. The seasonal change in stratospheric H_{eff} is relatively small (25.4 ± 1.8 km (2 standard deviations)). Seasonal actinic flux changes, however, result in larger variability in stratospheric NO_2 T_{eff} (Fig. 4) at these latitudes, especially in winter (Fig. 6). This is mainly due to polar weather effects.

We used GMI CTM outputs to evaluate whether stratospheric and tropospheric T can be estimated from temperature profiles (atmospheric soundings or model meteorological fields) at a specific altitude. Using stratospheric average $H_{eff} = 25.4$ km tends to underestimate stratospheric T_{eff} by 2.9 K and 5 K for the north-west USA and north-west Europe, respectively. This is probably the result of uncertainty in stratospheric lapse rate change around 25 km due to O_3 peak. Using average temperature between 20 and 30 km reduces some noise but still produces an offset of 4 K. Figure 5 shows difference between T_{eff} and temperature at 27 km which tends to have smaller errors in summer (1 to 2 K) and more significant error (up to 6 K) in winter. Annual differences (2011) between stratospheric T_{eff} and temperature at 27 km are 1 ± 1.6 K (north-west USA) and 2.8 ± 3 K (north-west Europe). Based on GMI simulations we conclude that temperature at 27 km ±3 K provides a good estimate of the $T_{vertical}^{STRAT}$ from April to October over middle latitude locations. Figure 5 also shows difference between GMI

tropospheric NO$_2$ T_{eff} and GMI surface temperature (10 m). Average difference (tropospheric $T_{eff} - T$ at 10 m) in summer is -5 ± 2.5 K which corresponds roughly to adiabatic lapse rate of 9.8 K km^{-1} (H ~ 0.5 km). Average annual differences in 2011 for northwest USA and north-west Europe are -3.8 ± 2.9 K and -3.7 ± 2.1 K respectively. Due to large GMI cell size and NO$_2$ emission spatial averaging actual tropospheric NO$_2$ profile temperature is probably closer to the surface temperature than GMI estimated. We conclude that $T_{vertical}^{TROP}$ can be approximated by temperature range from T at the surface ($T_{0\,km}$) to ($T_{0\,km} - 3$ K).

Figure 6 shows GMI CTM estimated total and stratospheric NO$_2$ profile T_{eff} for these two sites, where the offset between total and stratospheric T_{eff} is due to the tropospheric contribution. Moderately polluted north-west Europe has an offset of ~ 40 K, while clean continental north-west USA < 20 K.

5 TESEM summary

Table 1 summarizes steps to calculate total VCD at T and separate it into VCD^{TROP} and VCD^{STRAT} using assumptions about T^{TROP} and T^{STRAT}.

The main limitations of TESEM for separation of tropospheric and stratospheric column contributions are: (1) instrumental overall noise expressed as DOAS fitting optical depth residuals, (2) total ΔSCD at T, (3) tropospheric fraction of the total ΔSCD, (3) difference between tropospheric and stratospheric effective temperatures, and (5) accuracy in estimation of tropospheric and stratospheric effective temperatures.

Error calculation of the resulting tropospheric and stratospheric NO$_2$ columns is done empirically by varying input parameters to TESEM within their estimated variability. PBL NO$_2$ temperature is expected to vary within -3 K, stratospheric – within ± 3 K. Measurement noise is accounted for by changing ΔSCD within $\pm$error(ΔSCD). Standard deviation of the resulting NO$_2$ VCDs is then reported as an overall NO$_2$ VCD error.

6 MFDOAS instrument description and DOAS analysis setup

6.1 MFDOAS instrument description

MFDOAS is a grating spectrometer system with a spectral resolution of 0.83 nm and over-sampling at 7.8 pixels per full width at half maximum (FWHM) covering 282–498 nm wavelength range. It is capable of direct sun and MAX-DOAS observations. A scientific grade CCD (Princeton Instruments: PIXIS 2kBUV, 512×2048) is coupled with a 300 mm focal length single path Czerny–Turner spectrograph (upgraded based on SpectraPro 2356), with a 400 groove mm^{-1} grating. The CCD is thermoelectrically cooled to $-70\,°C$ to reduce dark current noise. Photons in direct-sun and scattered-light modes are collected by a telescope through a 74 cm long sky collimator with a quartz window. A series of black anodized baffles inside the collimator help reduce scattering and entry of out of field of view (FOV) light into the spectrograph. Direct-sun light is guided into the 8 cm diameter spectralon integrating sphere by three folding mirrors. The integrating sphere assures uniform illumination of the spectrometer optics and minimizes the effect of FOV pointing inaccuracy. Depending on the operational mode (direct sun or sky view), the integrating sphere moves in and out of the spectrometer FOV. Before entering the spectrometer, light passes through two filter wheels that contain UV transmitting filters (Hoya U340) for removing visible light, depolarizers (Halbo Optics WDQ25), a plug to block all light for dark current measurements, a polarizer, and a UV absorbing filter (Schott WG345).

The light input optics and spectrometer/CCD detection system is enclosed in a temperature controlled box ($20 \pm 1\,°C$) which is placed on a Kipp and Zonen 2AP G sun tracker/positioner. After an initial instrument alignment, the sun position is determined using a solar ephemeris calculation. The pointing precision and accuracy of the instrument FOV are 0.05° and 0.1° respectively. Wavelength calibration was determined by measuring emission lines from different calibration (HgNe, Ne, Kr, Xe) and hollow-cathode lamps (Ag(Ne), Pt(A), Cr) as well as from solar Fraunhofer lines.

6.2 Data description and DOAS analysis setup

TESEM to derive slant profile effective temperature with the subsequent separation of stratospheric and tropospheric columns from DOAS measurements is applied to MFDOAS DS data collected during the May – August months. Here we present analysis of data collected at four northern middle latitude locations: two with moderate to high anthropogenic pollution and two with low pollution rates.

Table Mountain – JPL facility (JPL-TMF) is located in California, USA and is characterized by low NO_2 pollution levels due to high altitude ($\sim$ 2.3 km). On most days heavily polluted Los Angeles basin air is confined below 2.3 km. During afternoon hours, however, the PBL height is approaching JPL-TMF altitude and larger pollution amounts are present (Wang et al., 2010). Pullman, WA (home to Washington State University, WSU) is located in rural, wheat growing part of eastern Washington State. The main source of NO_x pollution is vehicular emissions produced by $\sim$ 30 000 population, with $\sim$ 20 000 student body. In this work we present data collected during summer months (July, August 2011) when most students were gone from Pullman WSU campus. As a result, the NO_2 levels are very close to continental background. Cabauw Experimental Site for Atmospheric Research, a rural site in the heart of the Netherlands, is characterized by relatively large regional NO_2 pollution. Observations during the Cabauw Intercomparison campaign for Nitrogen Dioxide Measuring Instruments (CINDI, June–July 2009, Piters et al., 2012) are presented here. NASA Goddard Space Flight Center (NASA/GSFC) is located in Greenbelt, MD, which is part of Baltimore–Washington metropolitan area (USA). This is an urban site with large NO_x emissions. Summary of the measurement site description including source of temperature profiles, campaign average temperatures at 27 km and at surface temperatures can be found in Table 2.

Depending on the goals of the individual field campaigns MFDOAS operated in different modes. In general, DS and MAX-DOAS measurements were taken in sequence. The interval between DS measurements depended on the number of MAX-DOAS elevation angles and directions. JPL-TMF campaign was devoted to intercomparison

between instruments in DS mode. As a result, high temporal resolution data are available (every minute). Measurements over WSU/Pullman and Cabauw sites had heavy emphasis on MAX-DOAS measurements, and, as a result DS data are available only every 15–20 min. Observations over NASA/GSFC again had high emphasis on DS measurements with DS visible NO_2 data available every 5 min.

Due to a difference in design (smaller telescope), the signal-to-noise ratio in data collected over JPL-TMF site was smaller than in measurements at other sites. The least favorable DS measurement conditions were observed at Cabauw because of measurement schedule and meteorological conditions. DS reference spectra were measured around local noon on 7 July 2007 for JPL-TMF, 4 July 2009 for Cabauw, 7 August 2011 for WSU/Pullman and 3 May 2013 for NASA/GSFC. To reduce noise propagation from the reference spectrum into DOAS analysis results, several spectra were averaged to create a single reference spectrum.

Table 3 lists all DOAS fitting parameters used to retrieve NO_2 ΔSCDs from MF-DOAS DS measurements. DOAS fitting was done by QDOAS software (Danckaert et al., 2012). In addition to deriving T from the visible measurements, we also conducted a "traditional" DOAS analysis using NO_2 cross section at a single temperature (238 K for JPL-TMF and WSU/Pullman sites, and 270 K for Cabauw and NASA/GSFC sites), and NO_2 cross sections at two temperatures (220 and 298 K).

T was derived using Vandaele et. al. (2003) linear regression model at $T_0 = 220$ K. Stratospheric NO_2 profile effective temperature was taken from atmospheric soundings or ozonesondes at 27 km. Tropospheric temperature was approximated as surface temperature.

7 Results

The main goal of this section is to demonstrate that TESEM accurately calculates total NO_2 ΔSCD at profile T and provides a reasonable estimation of stratospheric and tropospheric columns based on retrieved NO_2 slant profile effective temperature from DS

DOAS observations. It also compares DS DOAS retrievals from TESEM and traditional DOAS fitting methods.

7.1 NO$_2$ profile T, total, stratospheric and tropospheric NO$_2$ VCDs

Since the quality of the DOAS spectral fit greatly impacts the success of TESEM we first show the optical depths of gaseous absorbers fitted by QDOAS software for two sites: JPL-TMF and NASA/GSFC. JPL-TMF is a challenging site due low NO$_2$ total and tropospheric columns. NASA/GSFC on the other hand is characterized by large NO$_2$ tropospheric columns. Figure 7a shows QDOAS fit of DS data collected over JPL-TMF at $\sim$ 14:56 PST on 12 July 2007 in visible (435–485 nm) when total NO$_2$ ΔSCD is $\sim 5 \times 10^{15}$ molecules cm^{-2} with less than 50 % of it – tropospheric. Figure 7b shows similar plot for the same AMF (1.34, 09:12 EST on 17 May 2013) over NASA/GSFC where the total NO$_2$ ΔSCD is $\sim 1.3 \times 10^{16}$ molecules cm^{-2} with $\sim$ 80 % of it – tropospheric. Residual optical depth RMS at JPL-TMF is somewhat larger (1.35×10^{-4}) than at NASA/GSFC (8.85×10^{-5}) due to design improvement in MFDOAS. Figure 7 shows that DOAS analysis can separate temperature dependent NO$_2$ absorption at residual RMS characteristic to the MFDOAS instrument.

Figure 8 shows examples of derived total NO$_2$ profile T from direct sun MFDOAS measurements with time coincident surface temperatures and interpolated temperatures at 27 km over four sites. We selected one day with low NO$_2$ loading and one day with high NO$_2$ loading from each site. Difference in estimated T between measurements at times with high and low emissions can be as high as 20 K. Table 3 lists mean effective NO$_2$ profile temperatures retrieved at each site during selected periods. Temperature differences between estimated NO$_2$ total column T and stratospheric T were 17 ± 12 K over JPL-TMF, 27 ± 9 K over WSU/Pullman, 48 ± 7 K over Cabauw, and 39 ± 10 K over NASA/GSFC.

Total NO$_2$ ΔSCD calculated by the DOAS fitting algorithm (QDOAS) as a function of the direct sun AMF over JPL-TMF (July 2007), WSU/Pullman (July, August 2011) and

NASA/GSFC (May 2013) are shown in Fig. 9. It also includes the resulting stratospheric and tropospheric ΔSCD based on the derived effective NO_2 profile temperatures. There is a clear separation of the total NO_2 ΔSCD into stratospheric and tropospheric columns. It is especially pronounced in JPL-TMF and WSU/Pullman data, where morning and afternoon stratospheric NO_2 ΔSCD have different slopes due to different photolysis rates. More variability in stratospheric NO_2 over NASA/GSFC can be partially explained by more "dynamic" meteorological conditions over NASA/GSFC in May 2013 than over both JPL-TMF in July 2007 and WSU/Pullman in July–August 2011. Temperatures measured at 27 km over NASA/GSFC in May 2013 varied by 6–8 K from day to day compared to no more than 3 K over the two other sites.

Under low pollution and small changes in ΔSCD, TESEM sometimes overestimates tropospheric column fractions due to high sensitivity to assumed stratospheric and tropospheric temperatures, as well as higher errors in ΔSCD and $ΔSCDT_α$. The resulting errors in stratospheric VCDs are $\leq 1 \times 10^{15}$ molecules cm^{-2}. In this study we apply running average smoothing of the derived stratospheric vertical columns by 4 h periods, and then use these new stratospheric columns to recalculate tropospheric columns.

Figure 10 shows total, stratospheric and tropospheric NO_2 VCDs over four sites derived from MFDOAS DS NO_2 T shown in Fig. 8. Campaign average total NO_2 VCD over JPL-TMF was $(3.9 \pm 1.1) \times 10^{15}$ molecules cm^{-2}, with about 30 % of it tropospheric $((1.2 \pm 0.9) \times 10^{15}$ molecules cm$^{-2})$. Similar on average VCDs were observed over WSU/Pullman site $((4.0 \pm 0.8) \times 10^{15}$ total, $(1.0 \pm 0.7) \times 10^{15}$ molecules cm^{-2} tropospheric). Cabauw air was "polluted" almost on all days when DS measurements were available and an average total column was $(1.3 \pm 0.3) \times 10^{16}$, with $(9.5 \pm 3.2) \times 10^{15}$ tropospheric pollution. NASA/GSFC site had relatively clean and also highly polluted days depending on the day of week and wind direction. An average total observed column was $(8.8 \pm 3.5) \times 10^{15}$ and tropospheric $(5.6 \pm 3.5) \times 10^{15}$ molecules cm^{-2}. Derived stratospheric VCDs have a reasonable photolytic rate "slope" at all sites. The agreement between GMI CTM stratospheric VCD over WSU/Pullman site is within 6 % with linear correlation $R^2 = 0.92$.

7.2 Comparison of NO$_2$ ΔSCD derived from T fit and "traditional" fittings

The most common, "standard", approach is to estimate NO$_2$ T based on modeling results or in-situ measurements and apply this T along with the assumed NO$_2$ effective height to all of the measurements (Herman et al., 2009). In the case of JPL-TMF site estimated NO$_2$ profile T is 238 K, WSU/Pullman $\sim$ 240 K, Cabauw site $\sim$ 270 K, NASA/GSFC $\sim$ 270 K. In this study we linearly interpolate Vandaele et al. (2003) NO$_2$ cross sections at 220 K and 298 K to the desired temperatures. Fitting a constant temperature cross section results in biases that are pollution and temperature dependent. For polluted regions, during high NO$_2$ emission rates, the fixed temperature DOAS fitting underestimates ΔSCDs relative to TESEM, up to 5–10 %. While for the times with lower emission rates, the fixed temperature method overestimates ΔSCDs relative to TESEM by about 5–15 %. On average, the agreement is very good (within 1–6 %, Table 4) during summer months evaluated in this study. For sites with relatively constant NO$_2$ emission rates or background NO$_2$, the fixed temperature method is fairly accurate presuming the effective temperature is estimated correctly. Since a single T is used to analyze data independent of season systematic seasonal errors are expected even for such sites.

Second "standard" approach consists of simultaneous fitting NO$_2$ σ at assumed stratospheric (220 K) and tropospheric (298 K) temperatures. Two variations of this method exist: independent cross section fitting and "orthogonalised fitting". Since TESEM uses σ (NO$_2$) linear model derived from σ_{298K} and σ_{220K}, total ΔSCD (ΔSCD^{220K} + ΔSCD^{298K}) from the independent fitting of two cross sections is less than 1 % different than ΔSCD from TESEM.

"Orthogonalised fitting" is typically done in attempt to remove cross correlation between NO$_2$ cross sections at 220 K and 298 K (for which linear correlation is $\sim$ 0.99). The scaling factors, SF, in the 435–485 nm fitting window are 0.79 (σ_{298K} orthogonalised relative to σ_{220K}) and 1.26 (σ_{220K} orthogonalised relative to σ_{298K}). We found perfect correlation (R^2 = 1.000) between retrieved ΔSCD^{220K} and ΔSCD^{298K} using

"standard" fitting (simultaneous fitting of σ_{298K} and σ_{220K}) and "orthogonalised" fitting (simultaneous fitting of σ_{220K} and σ_{298K} orthogonalised relative to σ_{220K} and vise versa) for all sites. It is not clear what benefit NO_2 cross section orthogonalization of one temperature relative to the other presents for NO_2 retrieval from DS measurements at MFDOAS residual levels.

8 Conclusions

This paper presents a TEmperature SEnsitivity Method (TESEM) to more accurately calculate the total NO_2 column and atmospheric slant NO_2 profile weighted temperature (T), and to separate stratospheric and tropospheric columns from DS ground-based measurements using the retrieved T. TESEM is based on DOAS fitting of linear temperature dependent NO_2 absorption cross section (σ (T)) regression model (Vandaele et al., 2003). The direct result of the DOAS spectral fitting is NO_2 differential slant column density (ΔSCD) at the actual atmospheric NO_2 T. Atmospheric NO_2 T is determined from the DOAS fitting results after SCD in the reference spectrum is estimated using MLE.

Since NO_2 is mostly distributed between the lower troposphere and middle stratosphere and direct sun measurements have almost equal sensitivity to stratospheric and tropospheric absorption at solar zenith angles $< 75°$, the retrieved total NO_2 T can be represented as a sum of tropospheric fractions of the total SCD_{NO_2}. We use GMI CTM simulations to evaluate diurnal and seasonal variability of stratospheric and tropospheric NO_2 T over two middle latitude sites in 2011. GMI simulations reveal that stratospheric NO_2 T over middle latitudes can be relatively accurately estimated (error < 3 K) by the measured or simulated temperature at 27 km from April to October. The tropospheric NO_2 T can be approximated by the surface temperature.

TESEM was applied to the Washington State University Multi Function DOAS instrument (MFDOAS) measurements at four mid-latitude locations with low and moderate NO_2 anthropogenic emissions: (1) Table Mountain – Jet Propulsion Laboratory

(JPL-TMF) facility, CA (34.38° N/117.68° W); (2) Pullman, WA (46.73° N/117.17° W); (3) Greenbelt, MD (38.99° N/76.84° W) USA; and (4) Cabauw, the Netherlands (51.97° N/4.93° E) during summer months (July 2007, June–July 2009, July–August 2011, May 2013). NO$_2$ T, total, stratospheric and tropospheric NO$_2$ vertical columns were determined over each site.

Traditionally, either σ (NO$_2$) is fitted at a single estimated NO$_2$ T, or two predetermined (stratospheric and tropospheric) T. Use of a single T requires prior knowledge of the tropospheric–stratospheric NO$_2$ columns partitioning in the measurement. In addition, it assumes that this partitioning is constant throughout the measurement period (sometimes months). Fitting of two σ (NO$_2$) at fixed temperatures, typically 220 and 298 K, assumes constant stratospheric and tropospheric NO$_2$ T as a function of time. Neither assumption is correct, except as a convenient approximation. TESEM does not require prior knowledge of NO$_2$ effective temperatures during the DOAS fitting stage and retrieves T from the DOAS fitting results themselves.

For polluted regions, during high NO$_2$ emission rates, the fixed temperature method underestimates TESEM ΔSCDs, up to 5–10 %. While for the times with lower emission rates, the fixed temperature method overestimates TESEM ΔSCDs by about 5–15 %. On average, the agreement is very good (within 1–6 %) for all sites and short term campaigns during summer months. For sites with relatively constant NO$_2$ emission rates or background NO$_2$, the fixed temperature method is fairly accurate presuming the effective temperature is estimated correctly. Agreement between total ΔSCD resulting from the independent fitting of two NO$_2$ absorption cross sections at 220 and 298 K and ΔSCD from TESEM is very good (< 1 %). In case of cold months the traditional methods will require fitting NO$_2$ cross sections at the appropriate colder temperatures otherwise systematic errors are introduced. TESEM will need no adjustments.

Separation of stratospheric and tropospheric columns from DOAS measurements based on TESEM is mostly suited for measurements over regions where difference between total and stratospheric profile NO$_2$ temperatures and SCDs is large. In this study separation was successful with the corresponding temperature differences between

estimated NO_2 total column T and stratospheric T of $17 \pm 12\,K$ over JPL-TMF, $27 \pm 9\,K$ over WSU/Pullman, $48 \pm 7\,K$ over Cabauw, and $39 \pm 10\,K$ over NASA/GSFC.

Stratospheric and tropospheric NO_2 columns derived from simpler DS measurements are of great value to model and satellite data validation. Currently only total VCD are retrieved from DS measurements. Tropospheric DS NO_2 columns also can be used in MAX-DOAS inversion either as an initial guess or to "constrain" MAX-DOAS total tropospheric column retrieval. TESEM can also be applied to MAX-DOAS measurements to "subtract" stratospheric column from low elevation angles.

References

Bey, I., Jacob, D. J., Yantosca, R. M., Logan, J. A., Field, B. D., Fiore, A. M., Li, Q., Liu, H. Y., Mickley, L. J., and Schultz, M. G.: Global modeling of tropospheric chemistry with assimilated meteorology: model description and evaluation, J. Geophys. Res.-Atmos., 106, 23073–23095, doi:10.1029/2001JD000807, 2001.

Brewer, A. W., Mcelroy, C. T., and Kerr, J. B.: Nitrogen dioxide concentrations in the atmosphere, Nature, 246, 129–133, doi:10.1038/246129a0, 1973.

Butz, A., Bösch, H., Camy-Peyret, C., Chipperfield, M., Dorf, M., Dufour, G., Grunow, K., Jeseck, P., Kühl, S., Payan, S., Pepin, I., Pukite, J., Rozanov, A., von Savigny, C., Sioris, C., Wagner, T., Weidner, F., and Pfeilsticker, K.: Inter-comparison of stratospheric O_3 and NO_2 abundances retrieved from balloon borne direct sun observations and Envisat/SCIAMACHY limb measurements, Atmos. Chem. Phys., 6, 1293–1314, doi:10.5194/acp-6-1293-2006, 2006.

Cede, A., Herman, J., Richter, A., Krotkov, N., and Burrows, J.: Measurements of nitrogen dioxide total column amounts using a Brewer double spectrophotometer in direct Sun mode, J. Geophys. Res., 111, D05304, doi:10.1029/2005JD006585, 2006.

Chance, K. V. and Spurr, R. J. D.: Ring effect studies: Rayleigh scattering, including molecular parameters for rotational Raman scattering, and the Fraunhofer spectrum, Appl. Optics, 36, 5224–5230, doi:10.1364/AO.36.005224, 1997.

Clémer, K., Van Roozendael, M., Fayt, C., Hendrick, F., Hermans, C., Pinardi, G., Spurr, R., Wang, P., and De Mazière, M.: Multiple wavelength retrieval of tropospheric aerosol optical properties from MAXDOAS measurements in Beijing, Atmos. Meas. Tech., 3, 863–878, doi:10.5194/amt-3-863-2010, 2010.

Danckaert, T., Fayt, C., Van Roozendael, M., De Smedt, I., Letocart, V., Merlaud, A., and Pinardi, G.: QDOAS Software User Manual, Belgian Institute for Space Aeronomy (BIRA-IASB), 2012.

Douglass, A. R., Stolarski, R. S., Strahan, S. E., and Connell, P. S.: Radicals and reservoirs in the GMI chemistry and transport model: comparison to measurements, J. Geophys. Res.-Atmos., 109, D16302, doi:10.1029/2004JD004632, 2004.

Duncan, B. N., Strahan, S. E., Yoshida, Y., Steenrod, S. D., and Livesey, N.: Model study of the cross-tropopause transport of biomass burning pollution, Atmos. Chem. Phys., 7, 3713–3736, doi:10.5194/acp-7-3713-2007, 2007.

Fish, D. J. and Jones, R. L.: Rotational Raman scattering and the ring effect in zenith-sky spectra, Geophys. Res. Lett., 22, 811–814, 1995.

Frieß, U., Monks, P. S., Remedios, J. J., Rozanov, A., Sinreich, R., Wagner, T., and Platt, U.: MAX-DOAS O4 measurements: a new technique to derive information on atmospheric aerosols: 2. Modeling studies, J. Geophys. Res., 111, D14203, doi:10.1029/2005JD006618, 2006.

Grainger, J. F. and Ring, J.: Anomalous Fraunhofer line profiles, Nature, 193, 762, doi:10.1038/193762a0, 1962.

Harder, J. W., Brault, J. W., Johnston, P. V., and Mount, G. H.: Temperature dependent NO_2 cross sections at high spectral resolution, J. Geophys. Res., 102, 3861, doi:10.1029/96JD03086, 1997.

Heckel, A., Richter, A., Tarsu, T., Wittrock, F., Hak, C., Pundt, I., Junkermann, W., and Burrows, J. P.: MAX-DOAS measurements of formaldehyde in the Po-Valley, Atmos. Chem. Phys., 5, 909–918, doi:10.5194/acp-5-909-2005, 2005.

NO$_2$ direct sun DOAS measurements

E. Spinei et al.

Hendrick, F., Barret, B., Van Roozendael, M., Boesch, H., Butz, A., De Mazière, M., Goutail, F., Hermans, C., Lambert, J.-C., Pfeilsticker, K., and Pommereau, J.-P.: Retrieval of nitrogen dioxide stratospheric profiles from ground-based zenith-sky UV-visible observations: validation of the technique through correlative comparisons, Atmos. Chem. Phys., 4, 2091–2106, doi:10.5194/acp-4-2091-2004, 2004.

Hendrick, F., Pommereau, J.-P., Goutail, F., Evans, R. D., Ionov, D., Pazmino, A., Kyrö, E., Held, G., Eriksen, P., Dorokhov, V., Gil, M., and Van Roozendael, M.: NDACC/SAOZ UV-visible total ozone measurements: improved retrieval and comparison with correlative ground-based and satellite observations, Atmos. Chem. Phys., 11, 5975–5995, doi:10.5194/acp-11-5975-2011, 2011.

Herman, J., Cede, A., Spinei, E., Mount, G., Tzortziou, M., and Abuhassan, N.: NO_2 column amounts from ground-based Pandora and MFDOAS spectrometers using the direct-sun DOAS technique: intercomparisons and application to OMI validation, J. Geophys. Res., 114, D13307, doi:10.1029/2009JD011848, 2009.

Irie, H., Kanaya, Y., Akimoto, H., Iwabuchi, H., Shimizu, A., and Aoki, K.: First retrieval of tropospheric aerosol profiles using MAX-DOAS and comparison with lidar and sky radiometer measurements, Atmos. Chem. Phys., 8, 341–350, doi:10.5194/acp-8-341-2008, 2008.

Irie, H., Kanaya, Y., Akimoto, H., Iwabuchi, H., Shimizu, A., and Aoki, K.: Dual-wavelength aerosol vertical profile measurements by MAX-DOAS at Tsukuba, Japan, Atmos. Chem. Phys., 9, 2741–2749, doi:10.5194/acp-9-2741-2009, 2009.

Kattawar, G. W., Young, A. T., and Humphreys, T. J.: Inelastic scattering in planetary atmospheres. I – The Ring effect, without aerosols, Astrophys. J., 243, 1049–1057, 1981.

Kritten, L., Butz, A., Dorf, M., Deutschmann, T., Kühl, S., Prados-Roman, C., Pukite, J., Rozanov, A., Schofield, R., and Pfeilsticker, K.: Time dependent profile retrieval of UV/vis absorbing radicals from balloon-borne limb measurements – a case study on NO_2 and O_3, Atmos. Meas. Tech., 3, 933–946, doi:10.5194/amt-3-933-2010, 2010.

Li, X., Brauers, T., Shao, M., Garland, R. M., Wagner, T., Deutschmann, T., and Wahner, A.: MAX-DOAS measurements in southern China: 1. automated aerosol profile retrieval using oxygen dimers absorptions, Atmos. Chem. Phys. Discuss., 8, 17661–17690, doi:10.5194/acpd-8-17661-2008, 2008.

Li, X., Brauers, T., Shao, M., Garland, R. M., Wagner, T., Deutschmann, T., and Wahner, A.: MAX-DOAS measurements in southern China: retrieval of aerosol extinctions and validation

using ground-based in-situ data, Atmos. Chem. Phys., 10, 2079–2089, doi:10.5194/acp-10-2079-2010, 2010.

Li, X., Brauers, T., Hofzumahaus, A., Lu, K., Li, Y. P., Shao, M., Wagner, T., and Wahner, A.: MAX-DOAS measurements of NO_2, HCHO and CHOCHO at a rural site in Southern China, Atmos. Chem. Phys., 13, 2133–2151, doi:10.5194/acp-13-2133-2013, 2013.

Malicet, J., Daumont, D., Charbonnier, J., Parisse, C., Chakir, A., and Brion, J.: Ozone UV spectroscopy. II. Absorption cross-sections and temperature dependence, J. Atmos. Chem., 21, 263–273, doi:10.1007/BF00696758, 1995.

Martin, R. V.: Global inventory of nitrogen oxide emissions constrained by space-based observations of NO_2 columns, J. Geophys. Res., 108, 4537, doi:10.1029/2003JD003453, 2003.

McKenzie, R. L., Johnston, P. V., McElroy, C. T., Kerr, J. B., and Solomon, S.: Altitude distributions of stratospheric constituents from ground-based measurements at twilight, J. Geophys. Res., 96, 15499, doi:10.1029/91JD01361, 1991.

Mohnen, V. A.: The challenge of acid rain, Sci. Am., 259, 30–38, 1988.

Mount, G. H., Sanders, R. W., Schmeltekopf, A. L., and Solomon, S.: Visible spectroscopy at McMurdo Station, Antarctica 1. Overview and daily variations of NO_2 and O_3, Austral Spring, 1986, J. Geophys. Res., 92, 8320–8328, doi:10.1029/JD092iD07p08320, 1987.

Noxon, J. F.: Nitrogen dioxide in the stratosphere and troposphere measured by ground-based absorption spectroscopy, Science, 189, 547–549, doi:10.1126/science.189.4202.547, 1975.

Noxon, J. F., Whipple, E. C., and Hyde, R. S.: Stratospheric NO_2: 1. Observational method and behavior at mid-latitude, J. Geophys. Res., 84, 5047, doi:10.1029/JC084iC08p05047, 1979.

Olivier, J. G. J., Bouwman, A. F., Van der Hoek, K. W., and Berdowski, J. J. M.: Global air emission inventories for anthropogenic sources of NO_x, NH_3 and N_2O in 1990, Environ. Pollut., 102, 135–148, doi:10.1016/S0269-7491(98)80026-2, 1998.

Parrish, D. D.: Intercontinental Transport and Chemical Transformation 2002 (ITCT 2K2) and Pacific Exploration of Asian Continental Emission (PEACE) experiments: an overview of the 2002 winter and spring intensives, J. Geophys. Res., 109, D23S01, doi:10.1029/2004JD004980, 2004.

Piters, A. J. M., Boersma, K. F., Kroon, M., Hains, J. C., Van Roozendael, M., Wittrock, F., Abuhassan, N., Adams, C., Akrami, M., Allaart, M. A. F., Apituley, A., Beirle, S., Bergw-erff, J. B., Berkhout, A. J. C., Brunner, D., Cede, A., Chong, J., Clémer, K., Fayt, C., Frieß, U., Gast, L. F. L., Gil-Ojeda, M., Goutail, F., Graves, R., Griesfeller, A., Großmann, K., Hemeri-jckx, G., Hendrick, F., Henzing, B., Herman, J., Hermans, C., Hoexum, M., van der Hoff, G. R.,

Irie, H., Johnston, P. V., Kanaya, Y., Kim, Y. J., Klein Baltink, H., Kreher, K., de Leeuw, G., Leigh, R., Merlaud, A., Moerman, M. M., Monks, P. S., Mount, G. H., Navarro-Comas, M., Oetjen, H., Pazmino, A., Perez-Camacho, M., Peters, E., du Piesanie, A., Pinardi, G., Puentedura, O., Richter, A., Roscoe, H. K., Schönhardt, A., Schwarzenbach, B., Shaiganfar, R., Sluis, W., Spinei, E., Stolk, A. P., Strong, K., Swart, D. P. J., Takashima, H., Vlemmix, T., Vrekoussis, M., Wagner, T., Whyte, C., Wilson, K. M., Yela, M., Yilmaz, S., Zieger, P., and Zhou, Y.: The Cabauw Intercomparison campaign for Nitrogen Dioxide measuring Instruments (CINDI): design, execution, and early results, Atmos. Meas. Tech., 5, 457–485, doi:10.5194/amt-5-457-2012, 2012.

Plane, J. and Smith, N.: Atmospheric monitoring by differential optical absorption spectroscopy, in: Spectroscopy in Environmental Science, Vol. 24, Wiley, Chichester, 223–262, 1995.

Platt, U.: Differential Optical Absorption Spectroscopy (DOAS), in: Air monitoring by spectroscopic techniques, edited by: Sigrist, M. W., Vol. 127, Wiley-IEEE, New York, p. 531, 1994.

Platt, U., Perner, D., and Pätz, H. W.: Simultaneous measurement of atmospheric CH_2O, O_3, and NO_2 by differential optical absorption, J. Geophys. Res., 84, 6329, doi:10.1029/JC084iC10p06329, 1979.

Pommereau, J.-P. and Piquard, J.: Ozone and nitrogen dioxide vertical distributions by UV-visible solar occultation from balloons, Geophys. Res. Lett., 21, 1227–1230, doi:10.1029/94GL00389, 1994.

Preston, K. E., Jones, R. L., and Roscoe, H. K.: Retrieval of NO_2 vertical profiles from ground-based UV-visible measurements: method and validation, J. Geophys. Res., 102, 19089–19097, 1997.

Richter, A.: Absorptionsspektroskopische Messungen stratospharischer Spurengase uber Bremen 53° N, Ph.D. thesis, University of Bremen, Germany, available at: http://www.doas-bremen.de/publications.htm#pPhD (last access: 19 May 2014), 1997.

Rienecker, M. M., Suarez, M., Todling, R., Bacmeister, J., Takacs, L., Liu, H.-C., Gu, W., Sienkiewicz, M., Koster, R., Gelaro, R., Stajner, I., and Nielsen, J.: The GEOS-5 data assimilation system – documentation of versions 5.0.1, 5.1.0, and 5.2.0, in: Technical Report Series on Global Modeling and Data Assimilation, Vol. 27., 2008.

Sinreich, R., Friess, U., Wagner, T., and Platt, U.: Multi axis differential optical absorption spectroscopy (MAX-DOAS) of gas and aerosol distributions, Faraday Discuss., 130, 153–164; discussion 241–264, 519–524, 2005.

NO_2 direct sun DOAS measurements

E. Spinei et al.

Title Page

Abstract	Introduction
Conclusions	References
Tables	Figures

◄ | ►|

◄ | ►

Back | Close

Full Screen / Esc

Printer-friendly Version

Interactive Discussion

Solomon, S., Schmeltekopf, A. L., and Sanders, R. W.: On the interpretation of zenith sky absorption measurements, J. Geophys. Res., 92, 8311–8319, doi:10.1029/JD092iD07p08311, 1987.

Spinei, E., Carn, S., Krotkov, N., Mount, G. H., Yang, K., and Krueger, A.: Validation of OMI SO_2 measurements in the Okmok volcanic cloud over Pullman, WA, July 2008, J. Geophys. Res, 115, D00L08, doi:10.1029/2009JD013492, 2010.

Strahan, S. E., Duncan, B. N., and Hoor, P.: Observationally derived transport diagnostics for the lowermost stratosphere and their application to the GMI chemistry and transport model, Atmos. Chem. Phys., 7, 2435–2445, doi:10.5194/acp-7-2435-2007, 2007.

Vandaele, A., Hermans, C., Simon, P., Carleer, M., Colin, R., Fally, S., Mérienne, M.-F., Jenouvrier, A., and Coquart, B.: Measurements of the NO_2 absorption cross-section from $42\,000\,cm^{-1}$ to $10\,000\,cm^{-1}$ (238–1000 nm) at 220 K and 294 K, J. Quant. Spectrosc. Ra., 59, 171–184, doi:10.1016/S0022-4073(97)00168-4, 1998.

Vandaele, A. C., Hermans, C., Fally, S., Carleer, M., Mérienne, M.-F., Jenouvrier, A., Coquart, B., and Colin, R.: Absorption cross-sections of NO_2: simulation of temperature and pressure effects, J. Quant. Spectrosc. Ra., 76, 373–391, doi:10.1016/S0022-4073(02)00064-X, 2003.

Wagner, T., Dix, B., Friedeburg, C. v., Frieß, U., Sanghavi, S., Sinreich, R., and Platt, U.: MAX-DOAS O4 measurements: a new technique to derive information on atmospheric aerosols – principles and information content, J. Geophys. Res.-Atmos., 109, 22205, doi:10.1029/2004JD004904, 2004.

Wagner, T., Burrows, J. P., Deutschmann, T., Dix, B., von Friedeburg, C., Frieß, U., Hendrick, F., Heue, K.-P., Irie, H., Iwabuchi, H., Kanaya, Y., Keller, J., McLinden, C. A., Oetjen, H., Palazzi, E., Petritoli, A., Platt, U., Postylyakov, O., Pukite, J., Richter, A., van Roozendael, M., Rozanov, A., Rozanov, V., Sinreich, R., Sanghavi, S., and Wittrock, F.: Comparison of box-air-mass-factors and radiances for Multiple-Axis Differential Optical Absorption Spectroscopy (MAX-DOAS) geometries calculated from different UV/visible radiative transfer models, Atmos. Chem. Phys., 7, 1809–1833, doi:10.5194/acp-7-1809-2007, 2007.

Wagner, T., Ibrahim, O., Shaiganfar, R., and Platt, U.: Mobile MAX-DOAS observations of tropospheric trace gases, Atmos. Meas. Tech., 3, 129–140, doi:10.5194/amt-3-129-2010, 2010.

Wang, S., Pongetti, T., Sander, S. P., Spinei, E., Mount, G. H., Cede, A., and Herman, J.: Direct sun measurements of NO_2 column abundances from Table Mountain, California: in-

NO$_2$ direct sun DOAS measurements

E. Spinei et al.

Title Page

Abstract | Introduction

Conclusions | References

Tables | Figures

|◄ | ►|

◄ | ►

Back | Close

Full Screen / Esc

Printer-friendly Version

Interactive Discussion

tercomparison of low and high resolution spectrometers, J. Geophys. Res., 115, D13305, doi:10.1029/2009JD013503, 2010.

Wenig, M., Spichtinger, N., Stohl, A., Held, G., Beirle, S., Wagner, T., Jähne, B., and Platt, U.: Intercontinental transport of nitrogen oxide pollution plumes, Atmos. Chem. Phys., 3, 387–393, doi:10.5194/acp-3-387-2003, 2003.

NO$_2$ direct sun DOAS measurements

E. Spinei et al.

Table 1. Summary of TESEM to calculate total VCD at T and separate it into VCD$^{\mathrm{TROP}}$ and VCD$^{\mathrm{STRAT}}$.

STEP	Equation/Method		Important parameters
1. DOAS fitting of NO$_2$ abs. cross section linear model: constant (σ_0) and slope (α)	Non-linear least squares fitting (QDOAS in this study) $\Delta SCD = SCD - SCD^{REF}$	ΔSCD $\Delta SCDT_\alpha$ SCD	– differential slant column density at actual atmospheric slant profile weighted temperature [molecule cm^{-2}]; $= SCD^{REF} \cdot (T - T^{REF}) + \Delta SCD \cdot T$ [molecule K cm^{-2}] – NO$_2$ column along average photon path in the measured spectrum [molecule cm^{-2}]
2. Estimation of total NO$_2$ SCD in the reference spectrum	VCD^{REF} from Minimum Langley Extrapolation (MLE) method $SDC^{REF} = VCD^{REF} \cdot AMF^{REF}$	SCD^{REF} VCD^{REF} AMF^{REF}	– total SCD in the reference spectrum [molecule cm^{-2}]; – vertical column density in the reference spectrum; – air mass factor of the average photon path in the reference spectrum
3. Estimation of stratospheric NO$_2$ SCD in the reference spectrum	$T \approx \frac{\Delta SCDT_\alpha}{\Delta SCD}$; $AMF_{norm}^{TROP} = AMF^{TROP}/AMF$ $AMF_{norm}^{STRAT} = AMF^{STRAT}/AMF$ $T^{STRAT} = AMF_{norm}^{STRAT} \cdot T_{27\,km}$ $T^{TROP} = AMF_{norm}^{TROP} \cdot T_{0\,km}$ $\chi^{STRAT} = \frac{T - T^{TROP}}{T^{STRAT} - AMF^{TROP}}$ $\Delta SCD^{STRAT} \approx \Delta SCD \cdot \chi^{STRAT}$ VCD$_{REF}^{STRAT}$ from MLE $SDC_{REF}^{STRAT} = VCD_{REF}^{STRAT} \cdot AMF_{REF}^{STRAT}$	T $T_{0\,km}$ $T_{27\,km}$ χ^{STRAT} AMF_{norm}^{TROP} AMF_{norm}^{STRAT} T^{TROP} T^{STRAT} ΔSCD^{STRAT} VCD$_{REF}^{STRAT}$	– initial total slant NO$_2$ profile weighted temperature [K] for measurements with SCD$^{REF} \ll \Delta SCD$; – surface temperature [K]; – temperature at 27 km [K]; – stratospheric fraction of total SCD; – tropospheric air mass factor normalized by total AMF; – stratospheric air mass factor normalized by total AMF; – slant tropospheric NO$_2$ profile weighted temperature [K]; – slant stratospheric NO$_2$ profile weighted temperature [K]; – stratospheric SCD [molecule cm^{-2}]; – stratospheric VCD in the reference spectrum [molecule cm^{-2}]
4. Estimation of slant NO$_2$ T^{REF}	$T^{REF} = \frac{SCD_{STRAT}^{REF} \cdot T_{STRAT}^{REF} + SCD_{TROP}^{REF} \cdot T_{TROP}^{REF}}{SCD^{REF}}$	T^{REF}	– total slant NO$_2$ profile weighted temperature in reference spectrum [K];
5. Estimation of T	$T = \frac{\Delta SCDT_\alpha + SCD^{REF} \cdot T^{REF}}{SCD^{REF} + \Delta SCD}$	T	– final total slant NO$_2$ profile weighted temperature in reference spectrum for all measurements [K];
6. Estimation of stratospheric and tropospheric VCD	$\chi^{STRAT} = \frac{T - T^{TROP}}{T^{STRAT} - AMF^{TROP}}$; $\chi^{TROP} = 1 - \chi^{STRAT}$ $SCD^{STRAT} = (SCD^{REF} + \Delta SCD) \cdot \chi^{STRAT}$ VCD$^{STRAT} = SCD^{STRAT}/AMF^{STRAT}$	VCD^{STRAT} VCD^{TROP}	– stratospheric NO$_2$ VCD, [molecule cm^{-2}]; – tropospheric NO$_2$ VCD, [molecule cm^{-2}];

Table 2. MFDOAS measurement sites, observation periods and estimated stratospheric and tropospheric vertical NO$_2$ profile weighted temperatures.

Site name and location	Elev [m]	Dates	Source of temperature at 27 km[*]	Mean T at 27 km [K]	Mean T at surface [K]	Pollution level
Table Mountain – JPL facility, CA Lat: 34.38° N Lon: 117.68° W	2285	2–12 Jul 2007	Ozone sondes	225.84 ± 1.58	298.20 ± 3.04	low
WSU, Pullman, WA Lat: 46.7325° N Lon: 117.169° W	764	Jul, Aug 2011	Atm. soundings from Spokane, WA (47.68° N, 117.63° W)	227.29 ± 1.62	295.85 ± 4.33	low
Cabauw, the Netherlands Lat: 51.971° N Lon: 4.927° E	∼ 0	15 Jun–4 Jul 2009	Atm. soundings from DeBilt, the Netherlands (52.10° N, 5.18° E)	228.18 ± 1.65	296.41 ± 2.90	moderate–high
NASA/GSFC Greenbelt, MD Lat: 38.993° N Lon:76.839° W	∼ 60	May 2013	Atm. soundings from Sterling, VA (38.98° N, 77.46° W)	223.78 ± 2.13	293.37 ± 6.19	moderate–high

[*] Atmospheric soundings (http://weather.uwyo.edu/upperair/sounding.html) launched from nearby locations.

Table 3. DOAS fitting parameters used to analyze NO$_2$ visible direct sun data.

NO$_2$ visible fitting wavelength window: 435–485 nm
Reference spectra: local noon
Polynomial order: 4
Stray light correction: slope

Species	Abs. Cross Section Temperature [K]	Citation
O$_3$	223, 243	Daumont, Brion, Malicet (1995)
NO$_2$	(A) 298 and 220; (B) 270; (C) 238; (D) Derived T: linear model	Vandaele et al. (2003)
O$_2$O$_2$	296	Hermans et al., 2003 unpublished results http://spectrolab.aeronomie.be/o2.htm

Table 4. Table 4 MFDOAS measurement sites, observation periods and estimated total, stratospheric and tropospheric NO$_2$ effective temperatures.

Site name	Dates	Est. mean NO$_2$ T [K]	Measured mean NO$_2$ T [K]	NO$_2$ ($T - T_{27km}$) [K]	Slope/R^2 ΔSCD_{Tfixed} vs. ΔSCD_{TESEM}
TMF – JPL, CA (34.38° N, 117.68° W)	2–12 Jul 2007	238	243 ± 12	17 ± 12	0.941/0.998
WSU, Pullman, WA (46.73° N, 117.17° W)	Jul, Aug 2011	240	254 ± 9	27 ± 9	0.963/0.998
Cabauw, the Netherlands (51.97° N, 4.93° E)	15 Jun–4 Jul 2009	270	276 ± 7	48 ± 7	0.996/0.998
NASA/GSFC, Greenbelt, MD (38.99° N, 76.84° W)	May 2013	270	263 ± 10	39 ± 10	1.038/0.997

Title Page

Abstract | Introduction

Conclusions | References

Tables | Figures

|◄ | ►|

◄ | ►

Back | Close

Full Screen / Esc

Printer-friendly Version

Interactive Discussion
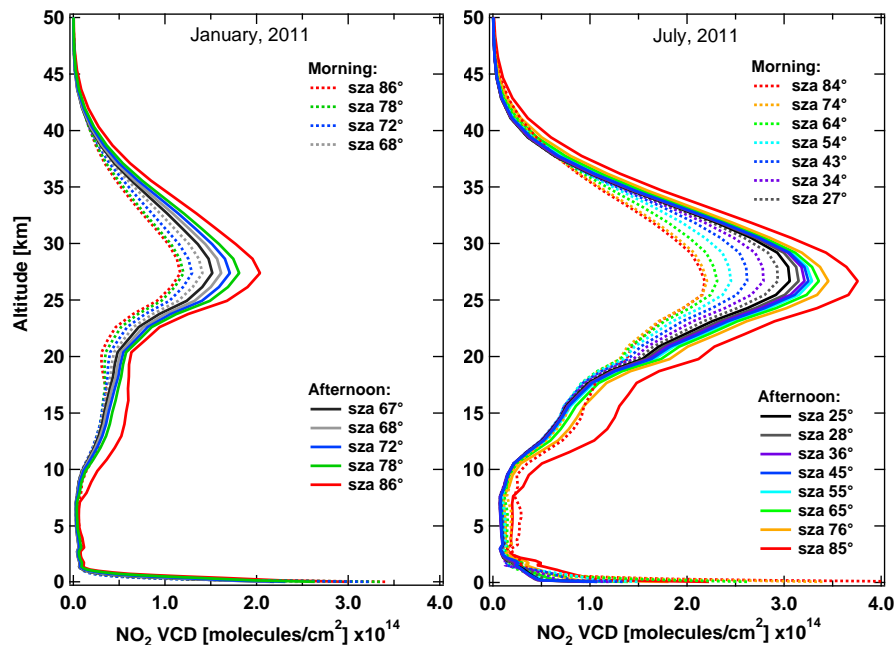
Figure 1. NO$_2$ monthly-averaged hourly profile simulations by GMI CTM for January (left panel) and July (right panel) 2011 over north-west USA (46° N/117.5° W). Time of the simulation is expressed as solar zenith angle (sza) in the morning or afternoon.
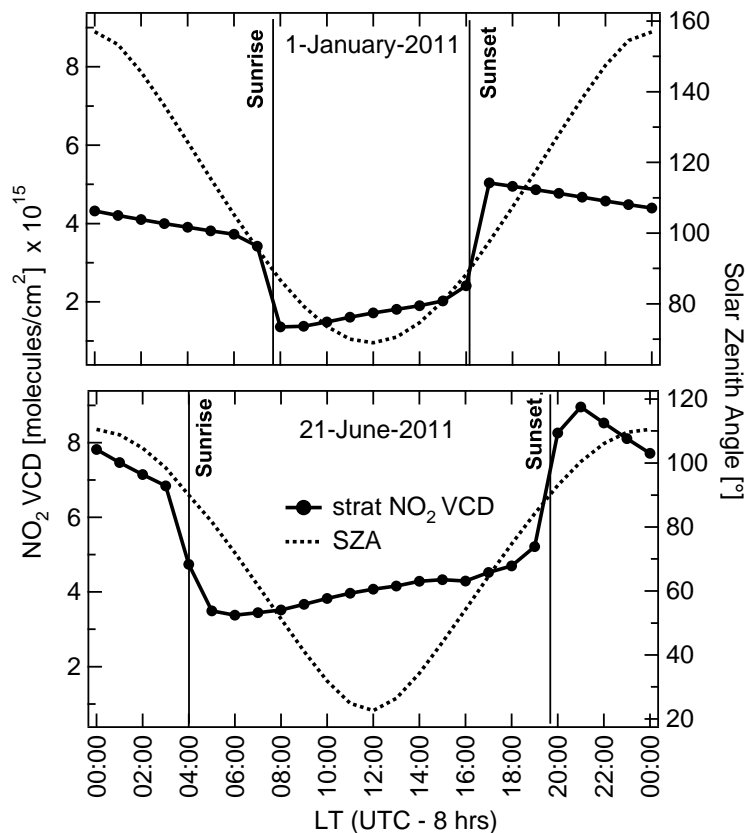
Figure 2. GMI CTM stratospheric NO$_2$ diurnal column variation estimates for 1 January 2011 (top panel) and 21 June 2011 (lower panel) over north-west USA (46° N/117.5° W).
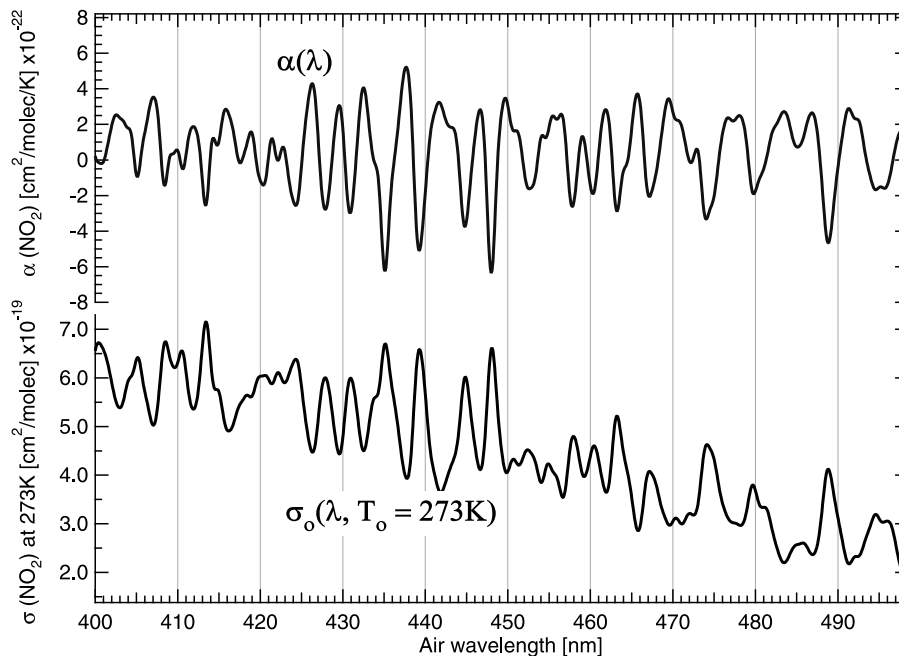
Figure 3. NO$_2$ absorption cross section linear regression model parameters $\sigma_0(\lambda)$ and $\alpha(\lambda)$ for $T_0 = 273\,\mathrm{K}$ derived by Vandaele et al. (2003) and convolved with MFDOAS instrument transmission function (FWHM = 0.83 nm).

Full Screen / Esc

Printer-friendly Version

Interactive Discussion
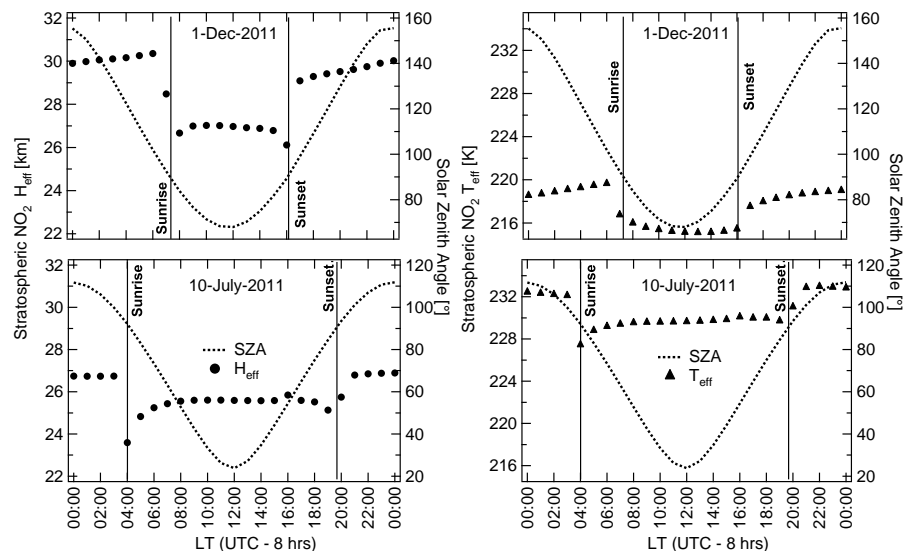
Figure 4. GMI CTM stratospheric NO$_2$ column estimations for 1 December 2011 (top panel) and 10 July 2011 (lower panel) over north-west USA (46° N/117.5° W). Diurnal stratospheric NO$_2$ profile weighted heights (H_{eff}) are shown on the left side. Corresponding diurnal stratospheric vertical NO$_2$ profile effective temperatures (T_{eff}) are shown on the right side. Solar zenith angles are also plotted to relate GMI estimations to DOAS measurements. Instantaneous GMI output temperatures at 00:00, 06:00, 12:00 and 18:00 UTC were interpolated on 24 h grid.
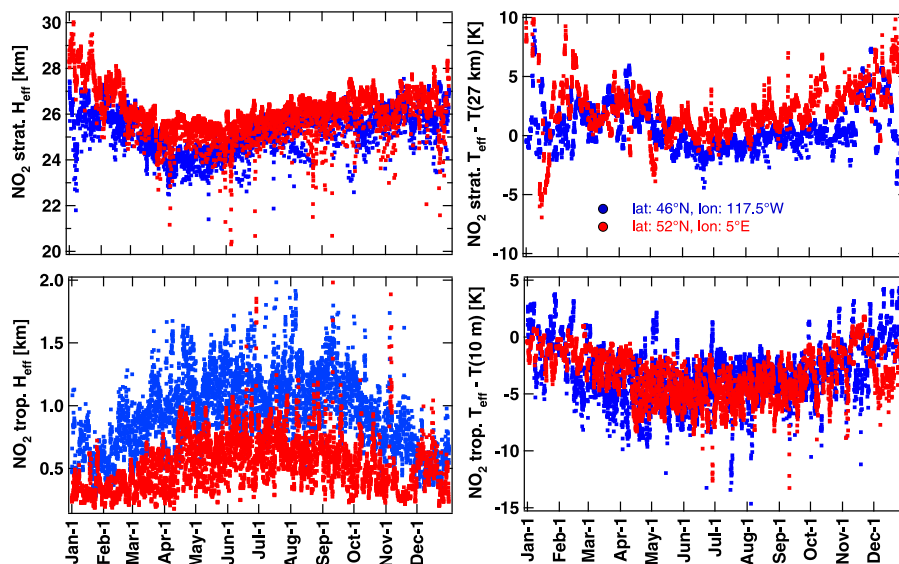
Figure 5. GMI CTM stratospheric NO_2 columns estimations for 2011 over north-west USA (46° N/117.5° W: blue) and north-west Europe (52° N/5° E: red) Seasonal stratospheric (upper left) and tropospheric (lower left) NO_2 profile effective heights (H_{eff}) are shown on the left panel. The difference between corresponding stratospheric NO_2 profile effective temperatures (T_{eff}) and temperature at 27 km are shown on the upper right panel. The difference between corresponding tropospheric NO_2 profile effective temperatures (T_{eff}) and temperature at 10 m above surface are shown on the lower right panel.
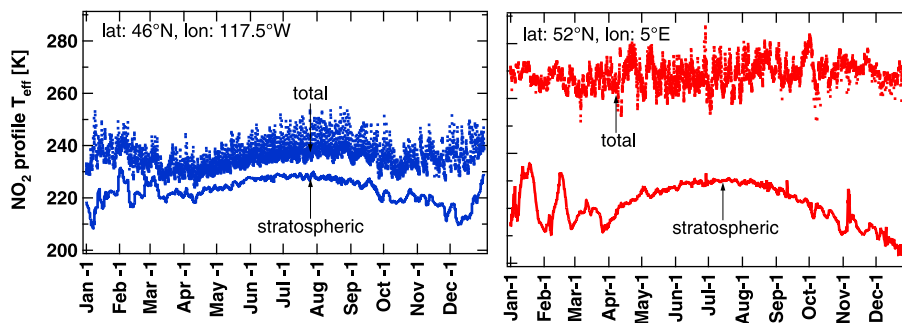
Figure 6. GMI stratospheric and total vertical NO$_2$ profile effective temperatures for 2011 over north-west USA (46° N/117.5° W, left) and north-west Europe (52° N/5° E, right). Only simulations for SZA $< 90°$ are plotted.
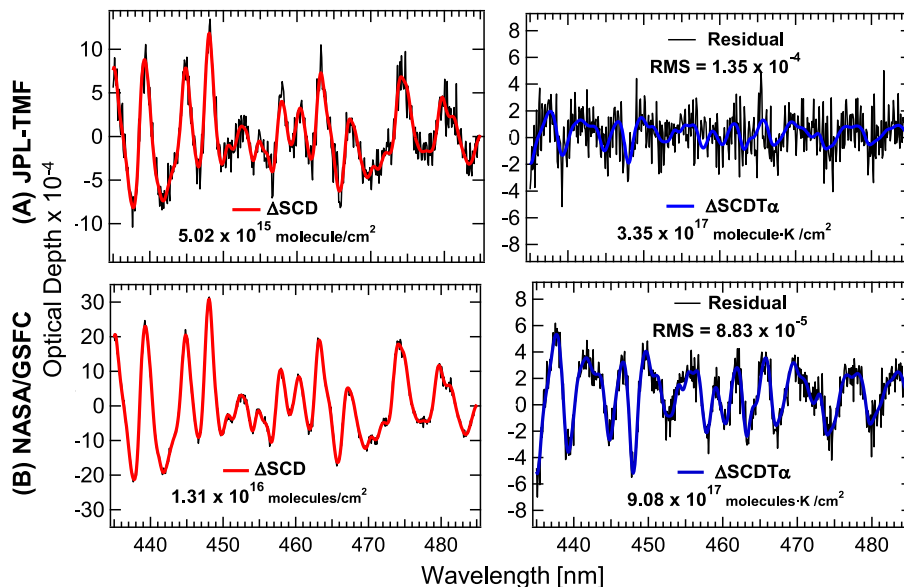
Figure 7. Example of DOAS spectral fit of retrieved NO$_2$ ΔSCD at T and ΔSCDTα from MFDOAS direct sun irradiance measurements (435–485 nm, $T_0 = 220$ K) over **(A)** JPL-TMF, California (~ 14:56 PST, 12 July 2007, reference taken at noon on 7 July 2007) and **(B)** NASA/GSFC (09:12 EST, 17 May 2013, reference taken at noon on 3 May 2013).
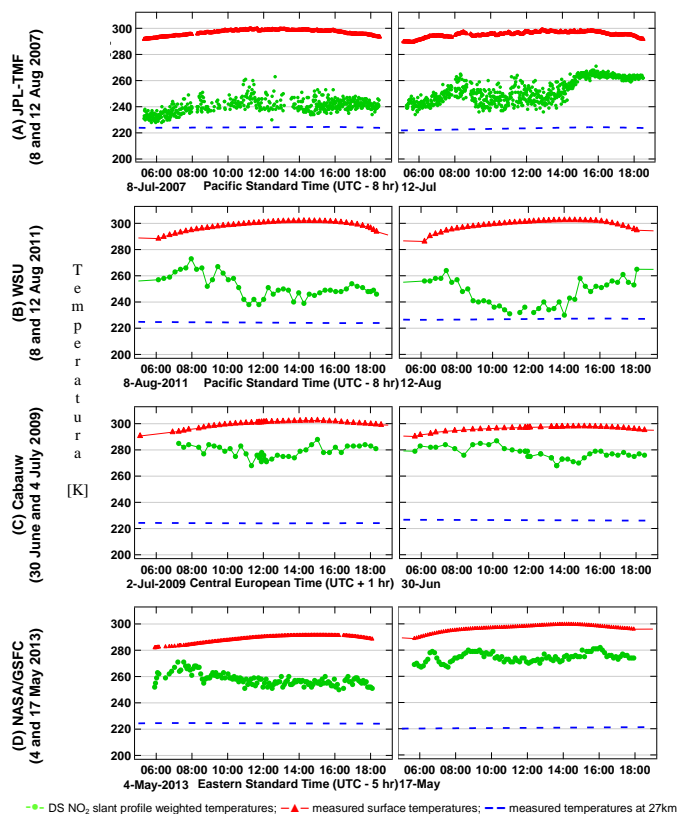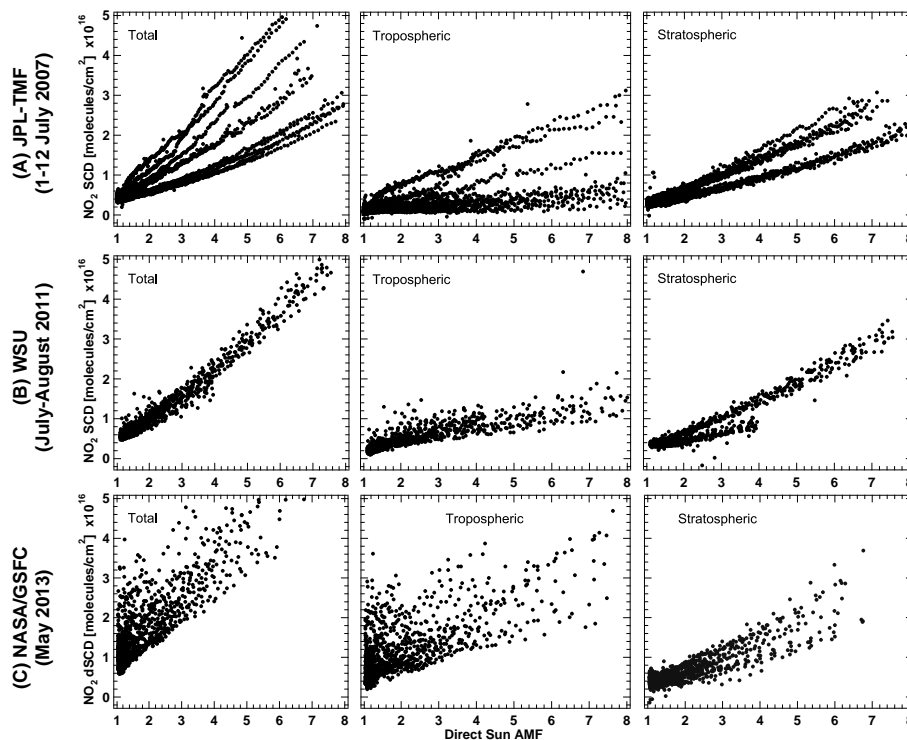
Figure 8. NO₂ slant profile weighted temperatures derived from MFDOAS direct sun measure-ments (435–485 nm) over two "clean" and two "polluted" sites: **(A)** JPL-TMF, California (8 and 12 July 2007), **(B)** WSU Pullman, WA (8 and 12 August 2001), **(C)** Cabauw, the Netherlands (30 June and 4 July 2009), and **(D)** NASA/GSFC Greenbelt, Maryland (4 and 17 May 2013).

Figure 9. NO$_2$ total, stratospheric and tropospheric SCDs derived from MFDOAS direct sun measurements (435–485 nm) over **(A)** JPL-TMF, California (2–12 July 2007), **(B)** WSU (July–August 2011), and **(C)** NASA/GSFC (1–31 May 2013). No smoothing of stratospheric columns is shown.
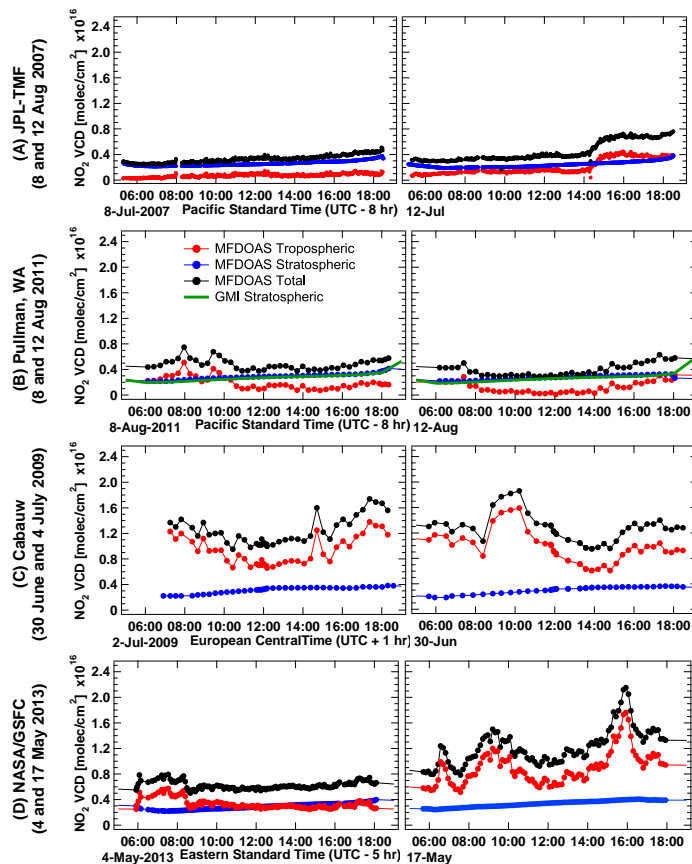
Figure 10. Total, stratospheric and tropospheric NO$_2$ VCDs derived from MFDOAS direct sun measurements (435–485 nm) over two "clean" and two "polluted" sites: **(A)** JPL-TMF, California (8 and 12 July 2007), **(B)** WSU/Pullman, WA (8 and 12 August 2001), **(C)** Cabauw, the Netherlands (30 June and 4 July 2009), and **(D)** NASA/GSFC Greenbelt, Maryland (4 and 17 May 2013).